Stokes drag and lubrication flows: A molecular dynamics study

Maxim Vergeles,[1] Pawel Keblinski,[1] Joel Koplik,[2] and Jayanth R. Banavar[1]
[1]*Department of Physics and Centre for Materials Physics, Pennsylvania State University, University Park, Pennsylvania 16802*
[2]*Benjamin Levich Institute and Department of Physics, City College of New York, New York, New York 10031*
(Received 4 December 1995; revised manuscript received 17 January 1996)

We have studied the translational and rotational motion of a sphere in a viscous Lennard-Jones liquid using molecular dynamics simulations. The drag and torque on a sphere in an effectively unbounded fluid are found to agree with continuum hydrodynamics results even when the size of the sphere is comparable to that of the fluid molecules. The diffusivity of a spherical tracer particle is in accord with the Stokes-Einstein relation, and the corresponding Brownian motion is determined by its interaction with the layers formed by fluid molecules around it. When a sphere moves near a solid wall, we find that the drag and torque agree with lubrication theory down to molecular scales, but the predicted divergence is regularized at very short distances due to depletion of fluid molecules near the wall and the appearance of slip at high shear stress. [S1063-651X(96)06005-9]

PACS number(s): 47.15.Gf

I. INTRODUCTION

The problem of a sphere slowly moving with a constant velocity in a viscous fluid (so that the Reynolds number is small, $\mathrm{Re}\ll 1$) is one of the most basic problems in hydrodynamics. For a sphere in an unbounded fluid it was solved by Stokes [1] in 1851, who obtained Stokes' law giving the force F acting on a sphere of a radius b moving with a velocity U in a fluid with viscosity μ:

$$F=6\pi\mu bU. \tag{1}$$

The exact solution of this problem using continuum hydrodynamics for a sphere in a semi-infinite fluid, bounded on one side by a solid surface was derived more than a century later by Brenner [2]. He obtained the following result for the case of a sphere moving perpendicular to the solid surface:

$$F=6\pi\mu bU\lambda, \tag{2}$$

with

$$\lambda=\tfrac{4}{3}\sinh\alpha\sum_{n=1}^{\infty}\frac{n(n+1)}{(2n-1)(2n+3)}\times\left[\frac{2\sinh(2n+1)\alpha+(2n+1)\sinh 2\alpha}{4\sinh^2(n+\tfrac{1}{2})\alpha-(2n+1)^2\sinh^2\alpha}-1\right],$$

$$\alpha=\cosh^{-1}(\epsilon)=\ln(\epsilon+[\epsilon^2-1]^{1/2}),$$

$$\epsilon=h/b+1,$$

where h is the minimal distance between the ball and the solid surface [Fig. 1(a)]. In the limit $h/b\to 0$ this expression reduces to

$$F=6\pi\mu Ub^2/h; \tag{3}$$

i.e., the force diverges when the sphere gets close to the solid surface.

This result, which is obviously inconsistent with our everyday experience, arises from several assumptions made in the analysis: (1) no-slip boundary conditions are valid, (2) the fluid density remains constant, even as the ball approaches the solid surface, and (3) both solid surfaces (of the ball and the wall) are assumed to be perfectly smooth.

No-slip boundary conditions have been employed in hydrodynamics for over a century now [3], and only recently has it been recognized that although there are many cases when they are sufficient, sometimes they lead to unphysical results. A classic example is the infinite energy dissipation predicted by hydrodynamics for the motion of a contact line separating two immiscible fluids along a solid surface [4]. In our falling ball problem, as the ball comes closer to the wall, the separation between its surface and the wall becomes smaller. The no-slip boundary condition requires a pressure gradient to displace the fluid from the gap between ball and wall, which diverges as the gap size vanishes. There are two possible factors that can prevent this divergence: first, a breakdown of the no-slip boundary conditions and, second, a depletion of the fluid in the gap between the wall and the ball.

Similar issues arise when one considers a sphere rotating in the vicinity of a wall. Calculations of Dean and O'Neill [5] and Goldman, Cox, and Brenner [6] give the following formula for the torque T acting from the fluid on a sphere rotating with an angular velocity Ω about an axis parallel to a solid surface at a distance h from it [Fig. 1(b)]:

$$T=8\pi\mu\Omega b^3 f(h/b),$$

$$x\to 0,\quad f(x)\sim\ln(x), \tag{4}$$

$$x\to\infty,\quad f(x)\to 1.$$

The function $f(x)$ cannot be obtained in closed form but can be evaluated to any desired accuracy by truncating a series expansion at the corresponding level.

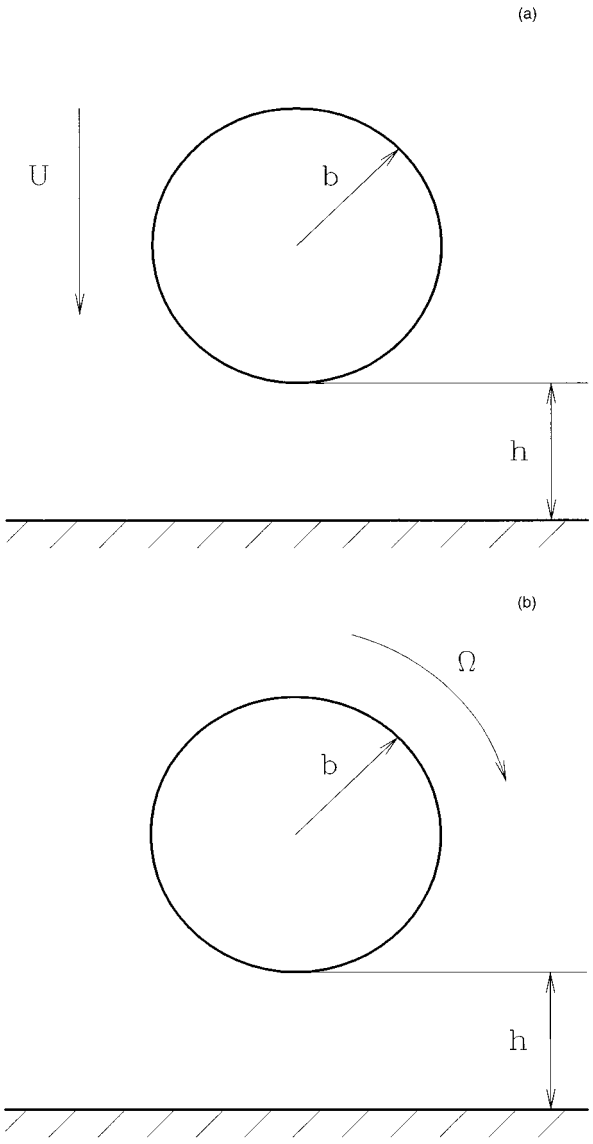

FIG. 1. (a) A sketch of a ball moving towards a solid surface. (b) A sketch of a ball rotating near a solid surface.

When the ball is far from the wall, $h \gg b$, one recovers the well known result for the sphere rotating in the unbounded fluid:

$$T = 8\pi\mu\Omega b^3. \tag{5}$$

In this paper we report the results of a study of these problems with the use of molecular dynamics (MD) simulations. The basic idea of MD simulations is the integration of Newton's equations of motion for the constituent molecules that interact with each other. Previous work has shown that even for small sizes and short times, the results of continuum theory are reproduced [7,8]. Nevertheless, since a continuum approximation is not made and the molecules are treated individually and in an *ab initio* manner, one may hope to effectively bridge the gap between microscopic and macroscopic phenomena. Alder, Alley, and Pollock [7] carried out MD simulations for hard spheres and showed that on introducing a nonlocal viscosity, Stokes' law (1) holds even for spheres whose radii are comparable with a molecular radius. Our results, obtained in a different context, are in accord with those of the earlier studies.

II. MOLECULAR DYNAMICS

We have used a standard MD algorithm in which molecules interact via a pairwise Lennard-Jones potential:

$$V(r) = 4\epsilon\left[\left(\frac{r}{\sigma}\right)^{-12} - \left(\frac{r}{\sigma}\right)^{-6}\right]. \tag{6}$$

This potential with $\sigma = 3.4$ Å and $\epsilon/k_B = 120$ K, along with molecular mass $m = 40$ a.u., is known to successfully reproduce the properties of liquid argon [9]. The natural time unit is then given by $\tau = \sigma\sqrt{m/\epsilon} = 2.16\times10^{-12}$ sec. In the remainder of this paper all dimensional quantities given as pure numbers will be understood as multiplied by an appropriate combination of σ, ϵ, and m.

In our simulations Newton's equations of motion were numerically integrated using a fifth order predictor-corrector algorithm with a time step of 0.0025τ. The layered-linked cell algorithm [10] was implemented to speed up the code. In the majority of our runs we used a system of a size $12\times12\times24$, which contained 3136 fluid molecules. The temperature T was chosen to be 1.2 and the density of the fluid 0.8 to correspond to the liquid phase. Periodic boundary conditions were imposed on the system in two directions. In the third direction, the fluid was bounded by periodically connected molecular walls with an fcc structure, consisting of 648 molecules, interacting with each other, the fluid molecules, and the ball through a Lennard-Jones potential. The mass of the wall molecules was chosen to be very large, so that they did not change their positions during the whole simulation. The lattice parameter of the walls was chosen to be 1.256σ [the nearest neighbor distance between wall molecules is $(1.256/\sqrt{2})\sigma$] and was incommensurate with the intermolecular interaction length of the fluid. The parameters of the Lennard-Jones potential for the fluid-solid interaction were chosen to be the same as that for the fluid-fluid interaction.

We have considered several models of the ball.

(1) Ball A: a spherical ball without inner structure, interacting with other particles through a modified Lennard-Jones potential:

$$V(r) = \begin{cases} 4\epsilon\left[\left(\dfrac{r-r_0}{\sigma}\right)^{-12} - \left(\dfrac{r-r_0}{\sigma}\right)^{-6}\right] & \text{if } r > r_0 \\ \infty \quad \text{if } r < r_0, \end{cases} \tag{7}$$

with $r_0 = 2.0$ in most of our runs.

(2) Ball B: a spherical ball with molecular structure. It was obtained by constructing a fcc lattice and taking the molecules that were inside a sphere of radius r_0. Each of the ball molecules interacted with other particles through a Lennard-Jones potential, with the same parameters as the fluid-fluid potential. Most of our simulations were carried out with a ball B1 consisting of $n = 56$ molecules, with the outer molecules being at a distance of $r_0 = 2$ from the center. We also considered two other balls, B2 with $r_0 = 3$ and $n = 56$ and B3 with $r_0 = 3$ and $n = 189$. The density of the ball B3 was the same as that of the ball B1.

Initially, the fluid molecules were placed at the vertices of a fcc lattice. For the temperature and density of the molecules, this configuration melted into a fluid phase. The whole system was equilibrated for 25τ. During this equilibration, the ball was maintained at a fixed position. After the system was equilibrated, the ball was set into motion at a constant speed U. Most of our data were obtained at $U=2$. We carried out some runs at $U=0.8$ to confirm that the qualitative results did not depend on the precise value of U. Typical values of the Reynolds number were $O(1)$. The mass of the ball A was chosen to be very large ($\sim 10^8$) in order to maintain the motion at constant speed. For ball B, the individual molecules were likewise chosen to be very heavy, thus maintaining the rigidity of the ball.

In order to study rotational motion we prepared the system as described above. After the initial equilibration the ball was rotated by assigning velocities $\mathbf{v}_i=\mathbf{\Omega}\times(\mathbf{r}_i-\mathbf{r}_c)$ to the individual molecules of the ball (we used only ball B to study rotational motion, since ball A does not have any structure and thus exerts no rotational drag on the surrounding fluid) at every time step, where $\mathbf{r}_c$ is the position of the center of mass of the ball and $\mathbf{r}_i$ is the coordinate of the ball molecule. We used $\Omega=1.2$ in our simulations.

III. STOKES LAW IN AN UNBOUNDED FLUID

We begin by addressing how well Stokes' law is reproduced at the microscopic scale of our MD simulations. To our knowledge, the only previous study of this problem was done by Alley and Alder [7]. They showed that generalized hydrodynamics quantitatively applies on the molecular scale by computing the dependence of the Stokes friction coefficient on the size of a massive Brownian particle.

We measured the force acting on a ball moving with constant velocity U in the central region of a large container of a viscous Lennard-Jones fluid with walls at the top and bottom and periodic boundary conditions in the transverse directions. [The net force was determined by a vector sum of the individual forces on the ball (or the molecules comprising the ball).] The container was chosen large enough that boundary effects did not play a role. Our attempts at using fully periodic boundary conditions without any walls led to a force that was somewhat smaller due to the effects of the replicas of the ball in the direction of motion (the effects of the replicas, perpendicular to the direction of motion, are not as large). Also the solid walls prevent the fluid from acquiring a nonzero mean velocity due to the momentum transfer from the ball. We extracted the effective ball radius (denoted by b_0) using (1). The force was averaged over 50 data points, each consisting of a time average over 0.25τ. The viscosity of the Lennard-Jones fluid under the conditions of our runs ($T=1.2$, $\rho=0.8$) has been measured previously in [8] and is equal to $\mu=1.94\pm0.16$. The results are given in Table I. They agree well with the definition of b as r_0+1. This definition comes from the observation that the effective radius of a particle in a solvent is the radius of the sphere inaccessible to the solvent particles [7]. Since the effective radius of the Lennard-Jones interaction is approximately 1, this radius should be r_0+1 in our case. To check this argument we performed simulations with a nonwetting ball A1, which interacted with fluid molecules only through the repulsive part of the modified Lennard-Jones potential (7). This ball had a larger effective radius than a regular ball A with the same r_0 (Table I), consistent with the definition of the effective radius as the radius of a sphere inaccessible to the solvent particles.

TABLE I. Effective radii b_0 [obtained from (1)], b_1 [from (5)], and b_2 [from (8)] for five different balls described in the text. The difference between b_0 and b_1 (or b_2) is a measure of the slip length for the rotational motion of the ball.

		b_0		b_1	b_2
Ball	r_0+1	$U=0.8$	$U=2.0$		
A	3.0	2.9 ± 0.3	3.3 ± 0.3		
A1	3.0	3.5 ± 0.4	3.6 ± 0.4		
B1	3.0	2.7 ± 0.3	3.1 ± 0.3	1.4 ± 0.2	1.7 ± 0.2
B2	4.0	4.5 ± 0.5	4.3 ± 0.4	2.2 ± 0.2	2.6 ± 0.3
B3	4.0	4.4 ± 0.5	4.3 ± 0.4	2.2 ± 0.2	2.7 ± 0.3

Likewise, to determine the effective radius of a rotating ball we measured the torque acting on a ball rotating in an unbounded Lennard-Jones fluid, and extracted the ball radius (denoted by b_1) using (5). (The net torque is the vector sum of the torques acting on the molecules comprising the ball, measured with respect to the center of mass.) The torque was averaged over 30 data points, each consisting of a time average over 2.5τ. The results are also shown in Table I. The effective radius is the same for B2 and B3 and thus independent of the ball density. The values of the effective radii are, however, quite different from our previous definition of b as r_0+1. To understand this difference one may consider the boundary conditions at the surface of rotating and translating balls. Both formulas (1) and (5) were obtained using an assumption that the fluid velocity near the ball surface equals the ball velocity. The translating ball pushes the fluid molecules below it, causing them to move with a velocity close to its own. Indeed, a significant fraction of the fluid surrounding the ball has to merely match the normal (to the ball) component of its velocity with that of the ball. As stated earlier the matching of the normal component of the fluid velocity with that of a solid is quite natural and should be expected.

On the other hand, in order to satisfy no-slip in the rotational case, the fluid surrounding a rotating ball needs to match the tangential component of its velocity with that of the ball. This requirement is more nontrivial and, indeed, one may not expect it to be valid on a microscopic scale. In order to study the boundary conditions on the surface of the rotating ball we measured the angular velocity of the fluid $\omega(r)$ as a function of a distance from the ball center r. According to hydrodynamics $\omega(r)$ obeys the equation

$$\omega(r)=\Omega b^3/r^3, \tag{8}$$

so that, on the ball surface ($r=b$), the angular velocity of the fluid equals the angular velocity of the ball Ω.

Figure 2(a) shows the angular velocity of the fluid, normalized by Ω versus $(r_0/r)^3$. To obtain this picture we divided the space around the ball into concentric spherical shells and averaged the ω in each shell for 100τ. It is obvious that no-slip boundary conditions are not satisfied [11], since

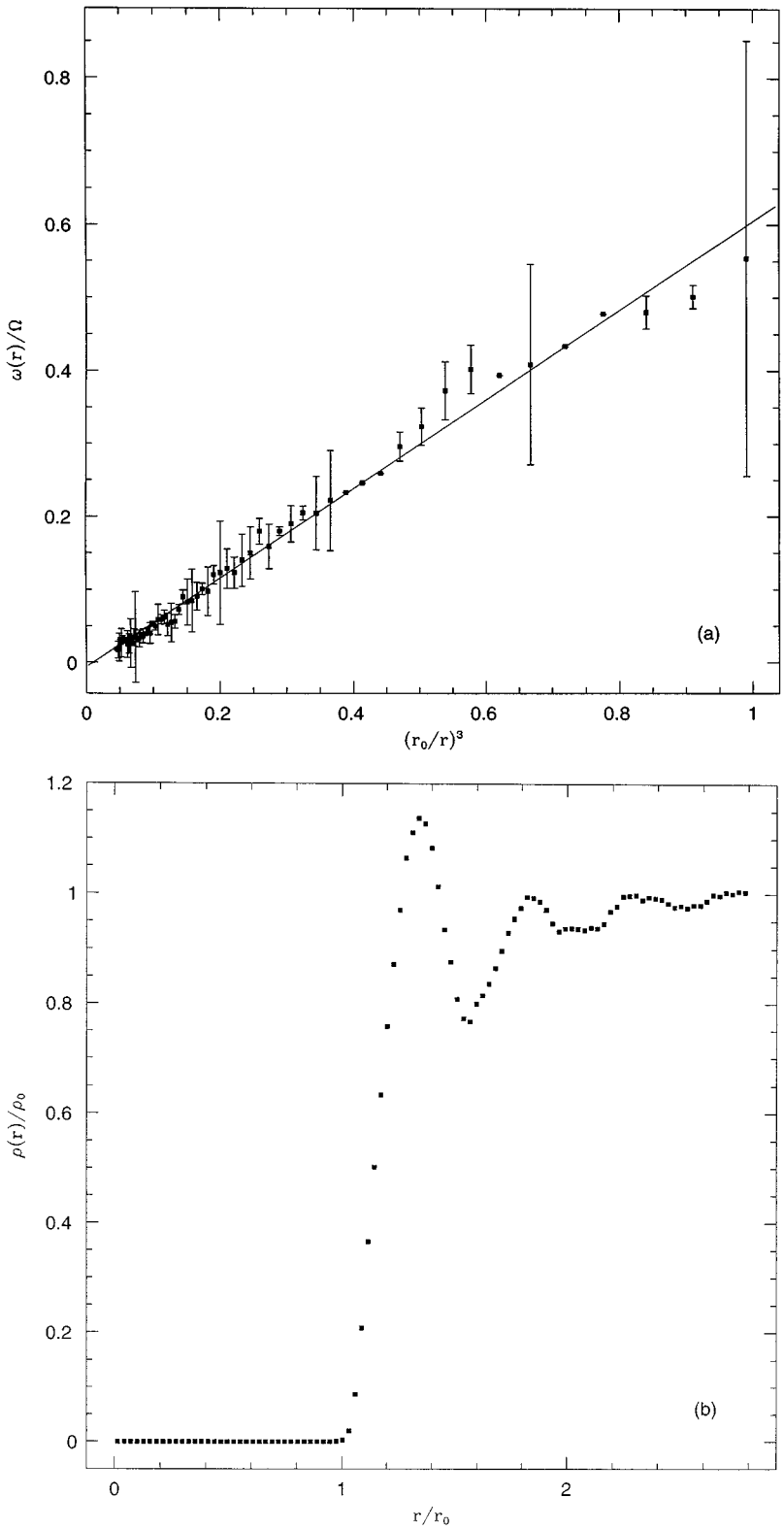

FIG. 2. (a) The angular velocity of the fluid, surrounding the rotating ball B1 ($r_0=2.0$, $\Omega=1.2$) as a function of the inverse cube of the distance from the center of the ball. The solid line is a least squares fit. The bars represent the statistical error estimates. (b) The fluid density near a rotating ball B1 ($r_0=2.0$, $\Omega=1.2$) showing the layering of the fluid around the ball.

at $r=r_0$, $\omega\approx 0.6\Omega$. One can obtain another estimate of the effective ball radius using (8) (we denote this value as b_2 in Table I). Estimates based on the slope of the curve [Fig. 2(a)] or on the value of b at which $\omega=\Omega$ lead to substantially the same results. The results show good agreement with the values of b_1 extracted from (5). Figure 2(b) shows a plot of the density of the fluid ρ around the rotating ball normalized by the mean fluid density ρ_0 versus (r/r_0). It is interesting to note that the rotation of the ball does not destroy layering. Further, the fluid density is indistinguishable from that around a nonrotating ball.

We also studied the translational motion of a spherical particle in a polymeric fluid. We used ball A in these studies. The molecules of the fluid were comprised of linear chains.

Each chain consists of 10 beads connected by an anharmonic spring [12]. All the beads interact via a pairwise repulsive Lennard-Jones potential

$$V(r)=\begin{cases} 4\epsilon\left[\left(\frac{r}{\sigma}\right)^{-12}-\left(\frac{r}{\sigma}\right)^{-6}+\frac{1}{4}\right] & \text{if } r\leqslant 2^{1/6}\sigma \\ 0 \quad \text{if } r\geqslant 2^{1/6}\sigma. \end{cases} \tag{9}$$

For the beads that are nearest neighbors in a chain, an additional attractive potential was added:

$$V_{atr}(r)=\begin{cases} -0.5kR_0^2\ln\left[1-\left(\frac{r}{R_0}\right)^2\right] & \text{if } r<R_0 \\ \infty \quad \text{if } r\geqslant R_0, \end{cases} \tag{10}$$

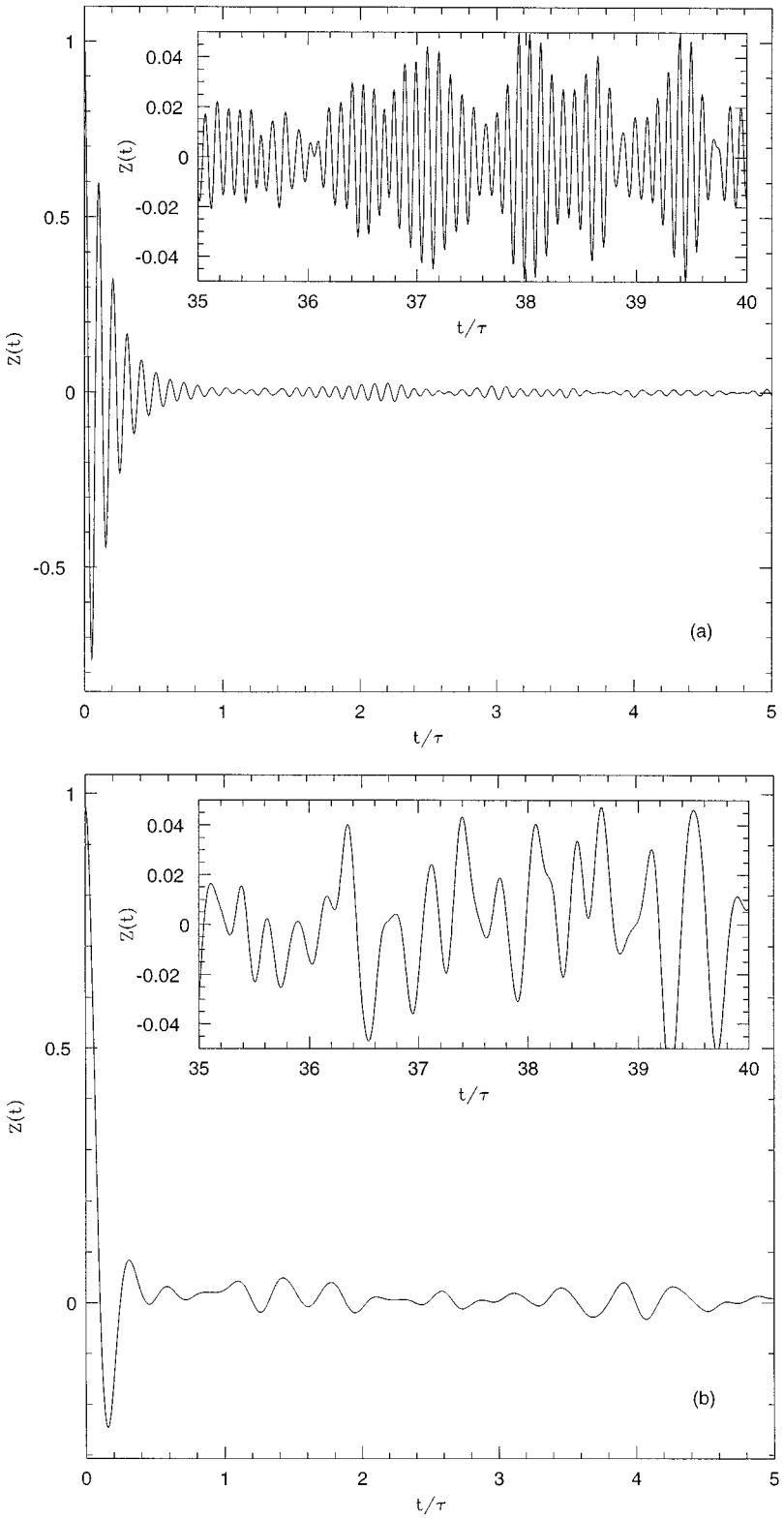

FIG. 3. The velocity autocorrelation function for balls (a) D1, (b) D2, and (c) D3. The inset shows the behavior at long times.

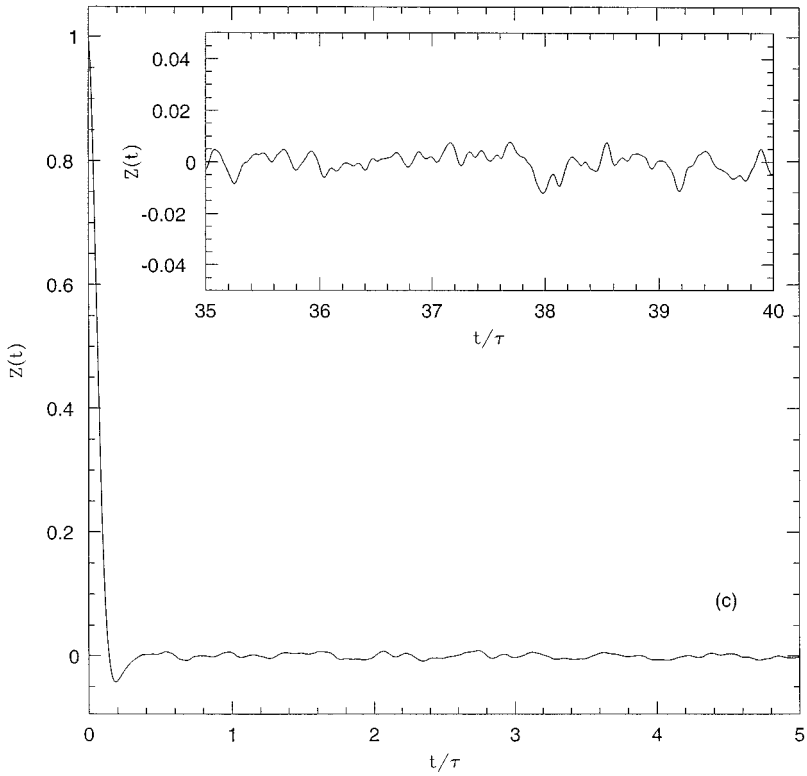

FIG. 3. (*Continued*).

with $R_0=1.5$ and $k=30$.

The chosen values of fluid density and temperature ($\rho=0.84$, $T=1$) correspond to the liquid phase. The radius of gyration of a polymeric fluid molecule is 2.8 ± 0.3. The viscosity of such a fluid was measured previously in [12]: $\mu=7.09\pm0.09$. We measured the force acting on a ball moving with a constant velocity through this fluid and extracted its effective radius b_p using (1). The results are given in Table II.

The difference between b_0 and b_p can be explained by the fact that since the molecules of the polymer are much larger than the ball, there should be a significant slip [it is interesting to note that the force acting on the Lennard-Jones particle ($r_0=0$) is the same, whether it moves through a Lennard-Jones or a polymeric fluid].

We conclude this section by noting that the discrepancies between the various length scales listed in Tables I and II, while clearly nonzero, are nevertheless of the order of a molecular diameter, so that in the large length scale limit, they would all effectively correspond to no-slip boundary conditions [13].

IV. DIFFUSION

The diffusion of a spherical particle in a viscous liquid is closely related to the problem of a particle moving with a constant velocity in the fluid. The simplest model describing the motion of such a particle is the Stokes-Einstein model, which gives the following mean square displacement of the diffusing particle at large time:

$$\langle \mathbf{r}^2(t)\rangle = 6Dt, \tag{11}$$

where

$$D = k_B T/(6\pi\mu b) \tag{12}$$

is the diffusion coefficient, which can also be related to the velocity autocorrelation function $Z(t)=\langle \mathbf{v}(0)\cdot\mathbf{v}(t)\rangle / \langle \mathbf{v}(0)\cdot\mathbf{v}(0)\rangle$.

$$D=\frac{k_B T}{m}\int_0^\infty Z(t)\,dt. \tag{13}$$

The first MD study of self-diffusion in liquid argon [14] showed that MD simulations can reproduce the properties of liquid argon quite well. In the present work we report the results of MD simulations of the diffusion of a tracer particle in a Lennard-Jones fluid. In these studies we used the ball A. The fluid molecules were initially placed at the vertices of a fcc lattice. Periodic boundary conditions were imposed on the system. After initial equilibration the ball was allowed to diffuse and its velocity was recorded at every time step (0.005τ).

Figure 3 shows the velocity autocorrelation function averaged over four runs for three different balls: Fig. 3(a): ball D1 with $r_0=3$ and $m=1$; Fig. 3(b): ball D2 with $r_0=3$, $m=10$; Fig. 3(c): ball D3 with $r_0=0$, $m=1$ [r_0 is defined in (7)]. Ball D3 was simply a tagged liquid molecule. Figure 4 shows the power spectrum $S(f)=\lim_{\tau\to\infty}|(1/\tau)\int_0^\tau dt\, Z(t)\exp(-ift)|^2$ of the velocity auto-

TABLE II. Effective radii obtained from (1) for the Lennard-Jones (b_0) and polymer (b_p) fluids.

r_0+1	b_0	b_p
1	0.52 ± 0.05	0.12 ± 0.01
4	$4.4\ \pm0.4$	$2.5\ \pm0.1$

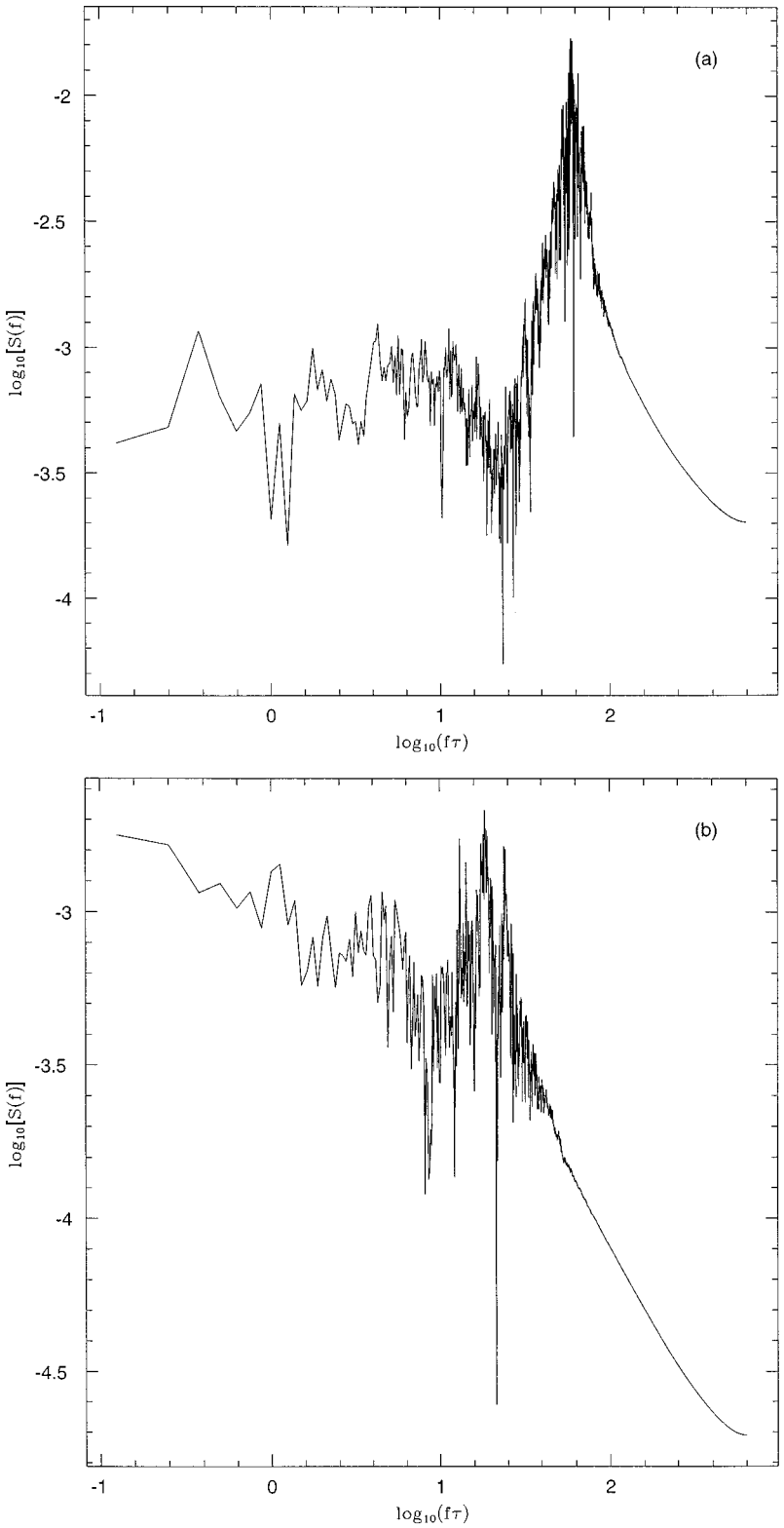

FIG. 4. The power spectrum of the velocity autocorrelation function for balls (a) D1, (b) D2, and (c) D3.

correlation function for the same three balls. Unlike that for ball D3, the velocity autocorrelation functions for balls D1 and D2 show oscillations that remain undamped even at relatively long times ($>40\tau$). The period T of these oscillations does not change with time and is related to the time t_1 when the velocity autocorrelation function becomes zero for the first time ($T=4t_1$). The amplitude modulation of the velocity autocorrelation function of ball D1 is presumably due to periodic boundary conditions.

To explain this behavior we focused on the liquid molecules that are close to the diffusing ball, since the ball motion is determined by the interaction with these molecules.

The fluid molecules form well pronounced layers around the ball. The time t_1 when the velocity autocorrelation function goes to zero for the first time can be estimated as a time t_s for the diffusing particle to stop after collision with a liquid molecule from the first layer, assuming that the liquid molecule does not move [15]. An explicit calculation gives

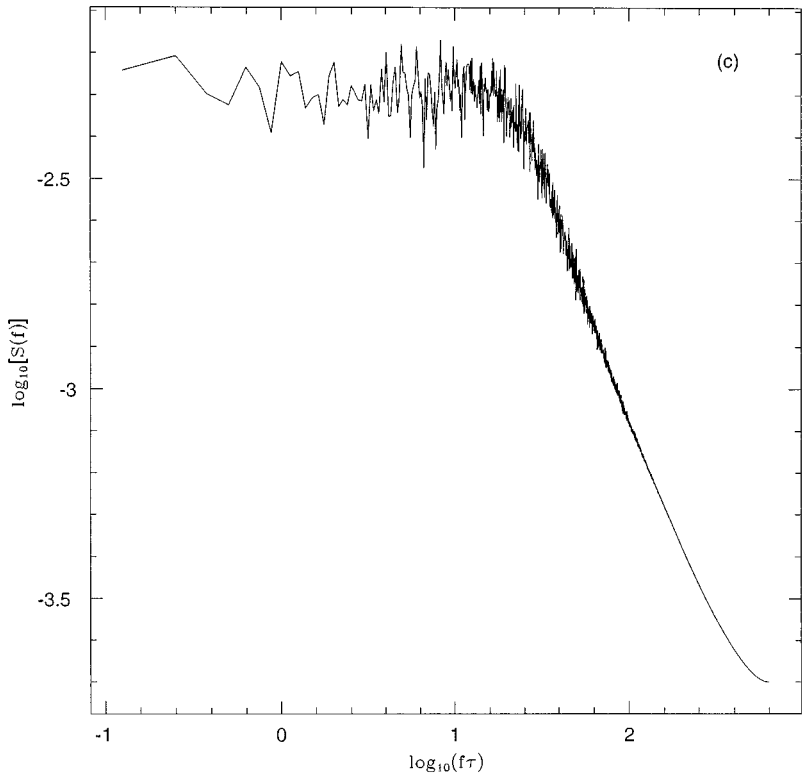

FIG. 4. (*Continued*).

$t_s = 0.025$, while $t_1 = 0.028$ for ball D1 and $t_1 = 0.145$ for ball D3. t_s estimates t_1 for D1 much better than for D3 because the larger the ball the better the approximation of the motionless liquid molecules.

Second, to see how stable the first layer is we performed the following simulation: we recorded the fluid particles that formed the first layer immediately after equilibration, then we calculated what fraction of those particles remained in the first layer at later times. Figure 5 shows that the first layer is much more stable in the case of ball D1 than in the case of ball D3, which should be expected since the number of the liquid molecules in the first layer around the ball D1 is much

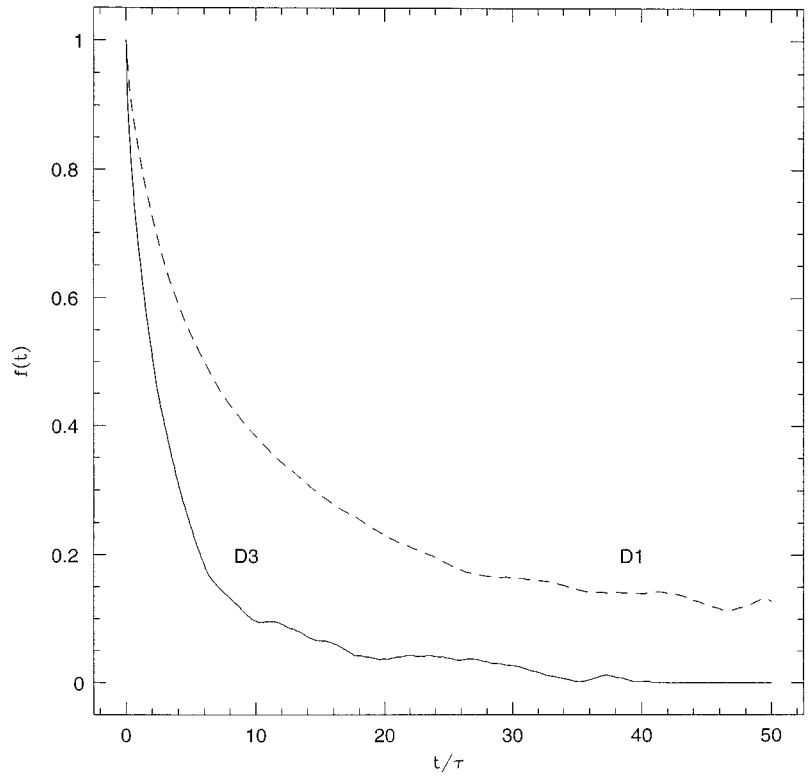

FIG. 5. The fraction $f(t)$ of the fluid molecules, which were in the first layer at $t = 0$, which remains in the first layer at time t for the balls D1 and D3.

TABLE III. Effective radii obtained from (1) (b_0) and (12) (b_D).

r_0+1	b_0	b_D
1	0.52 ± 0.05	0.41 ± 0.04
3	$2.9\ \pm0.3$	$1.9\ \pm0.2$
4	$4.4\ \pm0.4$	$2.7\ \pm0.3$

larger than around the ball D3. Figure 5 also shows that a significant fraction of the liquid particles that were in the first layer around ball D1 after equilibration remains there even at very long times ($\sim 50\tau$), which may explain the persistence of the oscillations.

We also calculated $Z_{bf}(t)=\langle \mathbf{v}(0)\cdot\mathbf{v_f}(t)\rangle/[\langle v^2(0)\rangle\langle v_f^2(0)\rangle]^{1/2}$, the correlation function of the velocities of the ball and the center of the mass of the first layer and the velocity autocorrelation function $Z_f(t)$ of the center of the mass of the first layer, enabling us to visualize the ball motion: it oscillates inside a cage [16] formed by the fluid molecules of the first layer, at the same time the cage itself moves more or less in one direction, since the velocity autocorrelation function of its center is positive.

The diffusion coefficient was calculated using (13). The diffusion coefficients obtained for balls D1 and D2 were the same, in agreement with (12). We extracted the effective radius of the ball using (12).

Table III presents the comparison between effective radii b_0 obtained from (1) and b_D from (12) for balls of different sizes. It is interesting to note that the effective radii obtained from (12) are somewhat smaller than those obtained from (1). This is due to the fact that although according to the Stokes-Einstein model the diffusing particle moves against the flow, on the average, in reality, it spends an equal amount of time moving with and against the cage, $Z_{bf}(t=0)\approx 0$, thus encountering less resistance.

V. STOKES' LAW IN THE PRESENCE OF A WALL

After studying the motion of the ball in the unbounded fluid we now turn to the problem of a sphere in the vicinity of a solid wall.

We first considered a ball translating in a fluid towards a molecular solid surface. Most of our results were obtained with ball A in these studies. A few runs with ball B1 yielded essentially the same behavior.

We define h, the distance from the ball to the wall, so that at $h=0$ the force of the wall on the ball vanishes. Our results are obtained from 10 runs, during each of which we averaged the force over 0.25τ, when the ball was far from the wall ($h>2.2$) and over 0.025τ, when the ball was close to the wall ($h<2.2$). Figure 6 shows the comparison between our MD simulations and the Brenner result (2). We find that the continuum results are reproduced until the separation between the ball and the wall becomes of the order of a few molecular radii.

In order to understand the origin of the discrepancy we focus on the behavior of the layer of fluid closest to the wall, as the ball comes very close to the wall ($h\approx 0$). Figure 7(a) shows the distribution of fluid molecules in the first layer, normalized by the mean fluid density, as a function of the horizontal distance from the center of the ball. In order to obtain this picture we divided the first layer into rings centered around the axis going through the ball center and perpendicular to the wall and averaged the number of fluid particles in each ring over 0.025τ in 34 independent runs. The

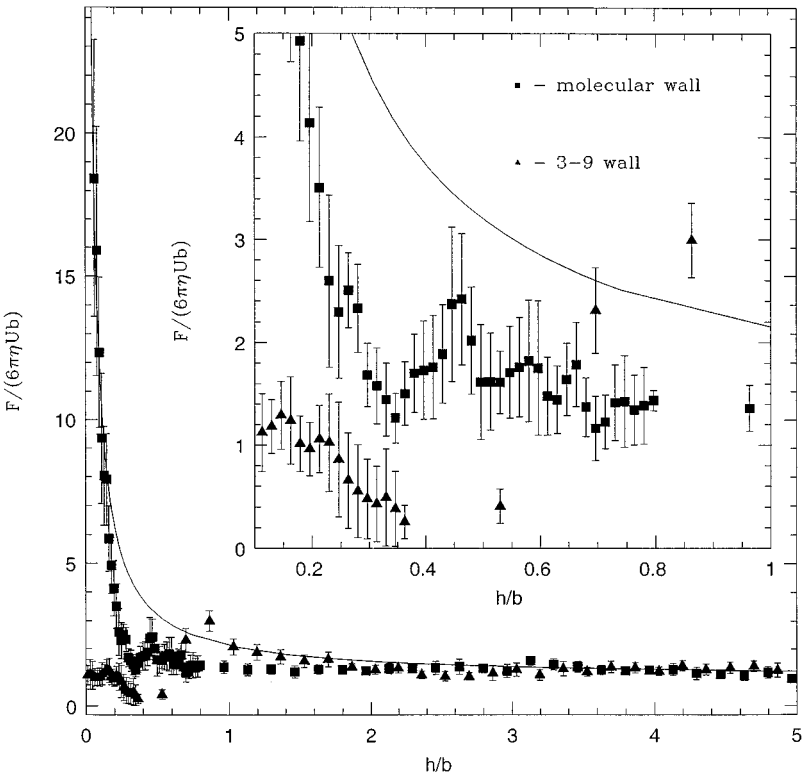

FIG. 6. The force of fluid resistance acting on ball A approaching a solid molecular or 3-9 potential wall, $U=2.0$, $b=3.0$. The solid line represents the Brenner result (2).

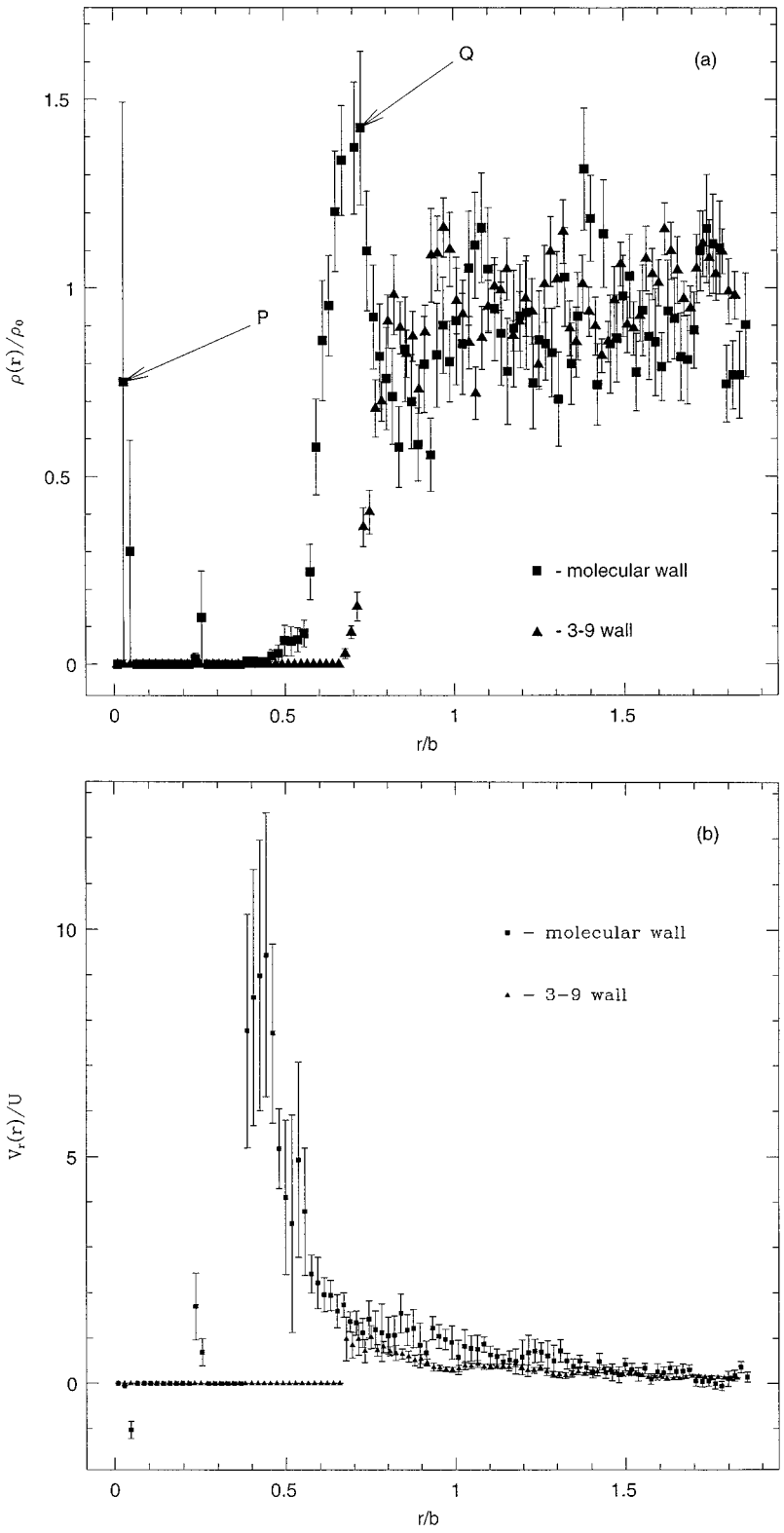

FIG. 7. (a) Density of the fluid in the first layer near the molecular and 3-9 potential wall, when the ball A ($b=3$, $U=2$) has just touched the wall. This picture was obtained by averaging over 34 runs; the point indicated by P corresponds to a total of 6 fluid molecules during all these runs, whereas the point indicated by Q corresponds to a total of 290 molecules. Note that the ring size corresponding to Q is larger than that for P. (b) Radial velocity distribution in the first layer of the fluid near the molecular and 3-9 potential wall, when ball A has just touched the wall. (c) Normal velocity distribution in the first layer of the fluid near the molecular and 3-9 potential wall, when ball A has just touched the wall.

figure indicates that, although the region under the ball is substantially depleted of fluid molecules, a few molecules remain trapped under the ball, whereas in equilibrium, this region is empty of all fluid molecules.

Figure 7(b) shows the breakdown of another assumption made in obtaining (2)—the validity of no-slip boundary conditions [17]. The figure is the plot of the radial velocity V_r normalized by the ball velocity U as a function of the radial distance from the ball center. It shows that fluid molecules have a nonzero radial velocity profile—they are being squeezed out from under the ball along the wall. At the same time, the normal component of the fluid molecules velocity V_z is essentially zero [Fig. 7(c)].

In order to assess how these results depend on the type of wall we are using, we also performed simulations with a continuum wall, obtained by replacing individual wall mol-

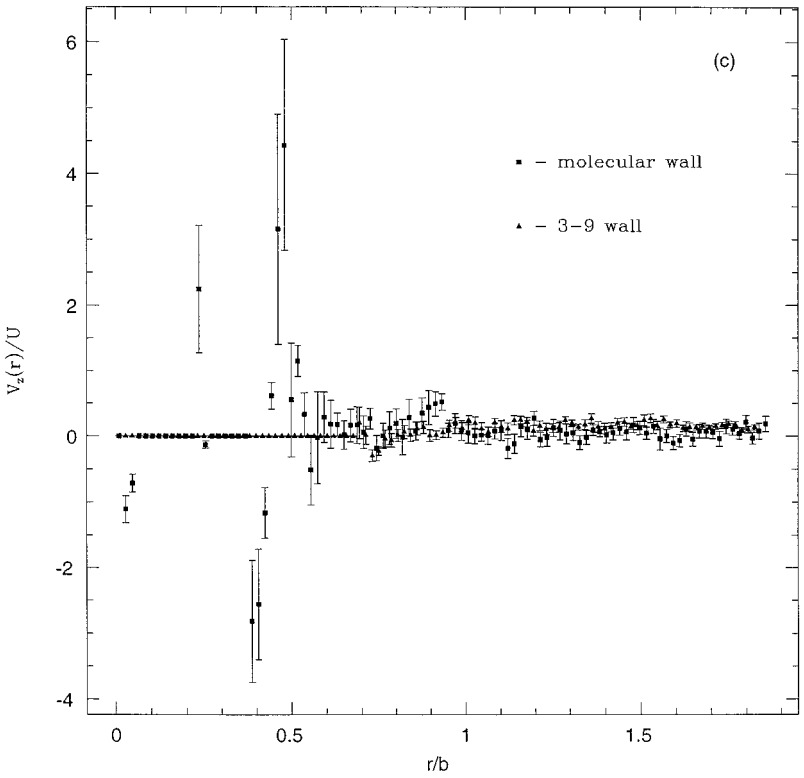

FIG. 7. (*Continued*).

ecules by a uniform density distribution, thus leading to a 3-9 potential in the direction perpendicular to the wall. Our results were obtained from 15 runs, during each of which we averaged the force over 0.25τ, when the ball was far from the wall ($h>2.2$) and over 0.025τ, when the ball was at a distance $h<2.2$ from the wall. Again, the force follows the continuum curve (2) until the ball-wall separation becomes of the order of a molecular radius (Fig. 6). In this case the force drops down earlier than in the case of the molecular wall. Since now the wall surface is smooth, it is much easier

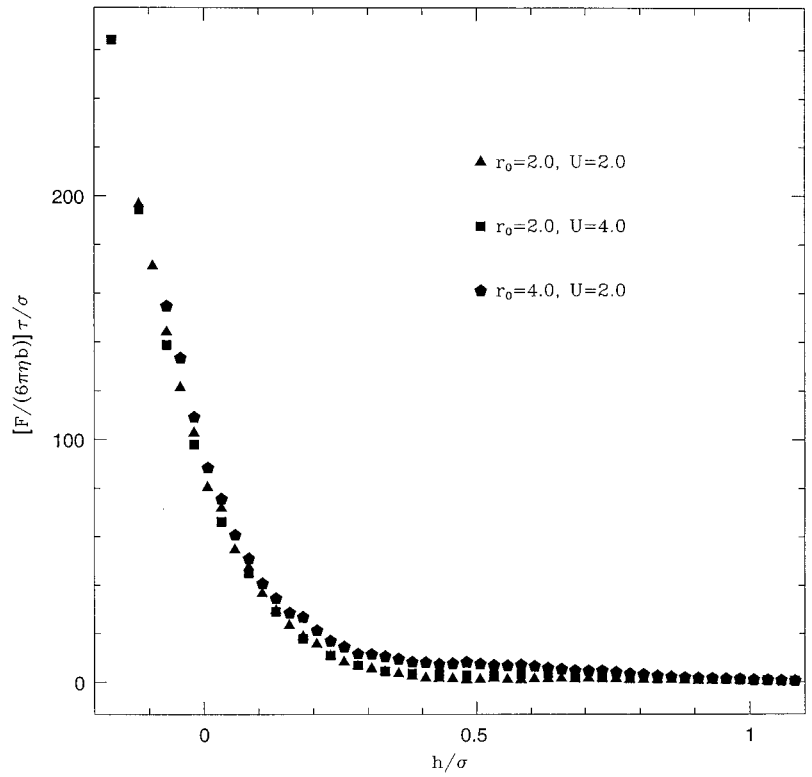

FIG. 8. The force of fluid resistance acting on ball A moving through a thin film of fluid for three different cases.

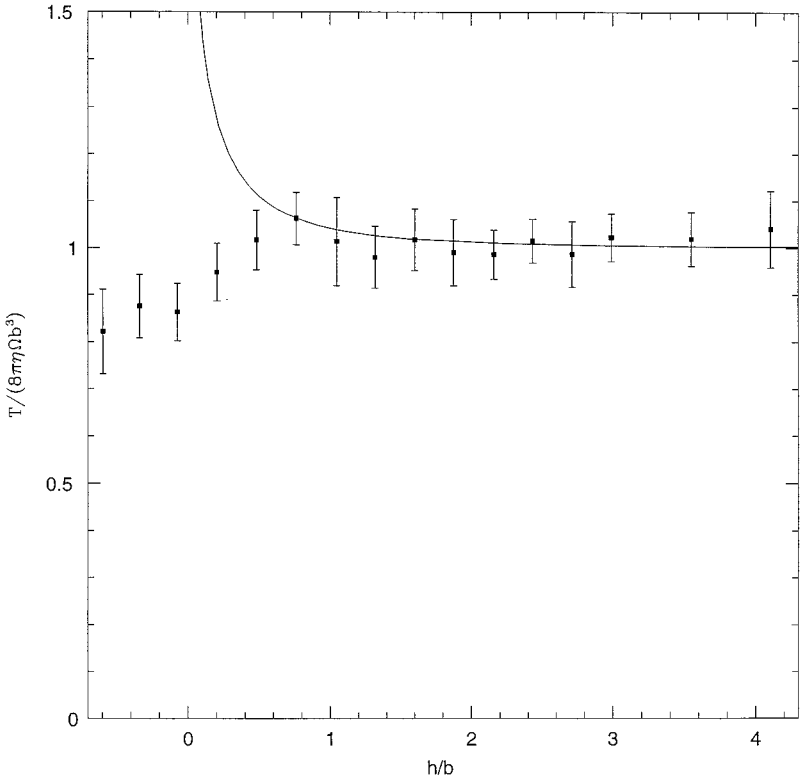

FIG. 9. The torque acting from the fluid on a rotating ball B1, $\Omega=1.2$, $r_0=2.0$. The solid line shows the predictions of Eq. (4).

to remove the fluid molecules from the gap between the ball and the wall. This can also be seen in Fig. 7(a), which shows the density distribution in the first layer of fluid molecules near the wall. The depleted region is larger than in the case of the molecular wall, and indeed, it is larger than the depleted region in an equilibrium situation, confirming the fact that it is easy to remove fluid molecules from under the ball in this case. Figure 7(b) shows that, again, no-slip boundary conditions are violated and there is a flux of fluid molecules away from the ball. The normal velocity is still close to zero [Fig. 7(c)]. It is interesting to note that the radial velocity in this case is of the order of the velocity of the ball, which is an order of magnitude smaller than for the molecular wall.

A simple explanation of this phenomenon is provided by the following analogy: one may consider a ball lying on a surface, which is pushed by some other object moving with constant velocity. If the surface is smooth and the ball does not get stuck it will move with the velocity of the pushing object; however, if the ball gets stuck (which is the case if the wall potential is corrugated because of the molecular structure) it will start to move later (the depletion region is smaller) and with much larger velocity when it is able to get depinned. Thus, we see that the breakdown of no-slip boundary conditions and the existence of a region depleted of fluid (leading to the removal of the divergence) do not qualitatively depend on the model of the wall being used.

We also performed MD simulations for the case when there is only a thin film (one molecular layer) of fluid adsorbed on a solid molecular wall. The results for ball A with $r_0=2.0$, $U=2.0$, $r_0=2.0$, $U=4.0$, and $r_0=4.0$, $U=2.0$ are shown in Fig. 8. We performed 15 runs for each ball, averaging the force over 0.025τ. This figure has two interesting features—first, the force takes on values that are much higher than in the semi-infinite fluid case and, second, the force does not depend on the ball velocity. Both these features can be explained by the fact that since the film is very thin, fluid molecules do not have enough time to get out of the way of the ball, and because of that the film acts almost like a rigid medium, which exerts a force, primarily depending on the displacement of its molecules and not on the velocity of the ball.

We now turn to a ball rotating in the vicinity of a wall. In these simulations a molecular wall was used. We used ball B1 in these studies, and we employed b_1 as an effective ball radius b. We placed our ball at a specified distance from the wall and rotated it at a constant angular velocity $\Omega=1.2$ and equilibrated the whole system for a period of 25τ. After this equilibration, we monitored the torque acting on the ball from the fluid. Figure 9 shows the torque T versus distance from the wall h. The values of the torque were averaged over 8 data points, each point representing an average over 12.5τ. The absence of a significant increase of the torque, let alone a logarithmic divergence as the ball approaches the wall, can be explained by a depletion of the fluid in the ball-wall gap. In our case the torque goes down rather than up because the ball has a smaller number of fluid molecules surrounding it.

VI. CONCLUSION

We have shown that MD simulations with a Lennard-Jones fluid can successfully reproduce the results of hydrodynamics such as (1) or (5) even for particles that are comparable in size to the fluid molecules. The only previous studies of this problem were performed by Alder, Alley, and Pollock [7], who used a fluid composed of hard spheres. Our results show that the effective radii of the moving balls, defined by formulas (1) and (5) are quite close to their geo-

metrical values. The effective radius of the translating ball can be defined as the radius of a sphere inaccessible to the solvent molecules. For the rotating ball the effective radius, entering (5), is smaller than the corresponding radius for translational motion. This discrepancy is due to the breakdown of no-slip boundary conditions on the surface of the rotating ball.

We have also studied the diffusion of a spherical particle in a Lennard-Jones fluid. We have shown that fluid molecules form well pronounced layers around the diffusing particle that are quite stable, and that determine the motion of the particle. The effective radii, entering (12), are somewhat smaller than those for translational motion due to the collective motion of the fluid molecules.

We have also addressed the issue of the unphysical divergences arising when two solid surfaces come close to each other. Our MD simulations show that if one takes into account the molecular aspects of the problem, the divergences are removed. We have also focused on the behavior of the fluid layer near the wall as the ball approaches the vicinity of the wall and monitored its density and velocity profile. The fluid between the ball and the wall is found to be depleted and no-slip boundary conditions are found to break down when the ball is close to the solid surface.

This work was supported by grants from NSF and NASA, the Pittsburgh Supercomputer Center, and the Center for Academic Computing at The Pennsylvania State University. We are grateful to Somnath Pal for useful discussions. J.R.B. acknowledges the warm hospitality of Alan Bray at the University of Manchester and Julia Yeomans at Oxford and support from the Fulbright Foundation and EPSRC.

[1] G. G. Stokes, Proc. Cambridge Philos. Soc. **9**, 8 (1851).
[2] H. Brenner, Chem. Eng. Sci. **16**, 242 (1961).
[3] J. C. Maxwell, Philos. Trans. R. Soc. London Ser. A **170**, 231 (1967).
[4] E. B. Dussan V and S. H. Davis, J. Fluid Mech. **65**, 71 (1974).
[5] W. R. Dean and M. E. O'Neill, Mathematica **10**, 13 (1963).
[6] A. J. Goldman, R. G. Cox, and H. Brenner, Chem. Eng. Sci. **22**, 637 (1967).
[7] W. E. Alley and B. J. Alder, Phys. Rev. A **27**, 3158 (1983); B. J. Alder, W. E. Alley, and E. L. Pollock, Ber. Bunsenges. Phys. Chem. **85**, 944 (1981).
[8] J. Koplik, J. R. Banavar, and J. F. Willemsen, Phys. Fluids A **1**, 781 (1989).
[9] J. P. Hansen and I. R. McDonald, *Theory of Simple Liquids* (Academic, New York, 1976).
[10] G. S. Grest, B. Dünweg, and K. Kremer, Comput. Phys. Commun. **55**, 269 (1989).
[11] The failure of no-slip boundary conditions for the rotational case had been observed earlier in J. Koplik and J. R. Banavar, Phys. Fluids A **5**, 521 (1993); **6**, 480 (1994).
[12] M. Kroger, W. Loose, and S. Hess. J. Rheol. **37**, 1057 (1993).
[13] The issue of boundary conditions of fluid flow past a solid surface in the channel geometry has been studied in detail by P. A. Thompson and M. O. Robbins, Phys. Rev. A **41**, 6830 (1990); see also L. Bocquet and J.-L. Barrat, Phys. Rev. E **49**, 3079 (1994); and J. Koplik and J. R. Banavar, Annu. Rev. Fluid. Mech. **27**, 257 (1995).
[14] A. Rahman, Phys. Rev. **136**, A405 (1964).
[15] B. Berne, J. Boon, and S. Rice, J. Chem. Phys. **45**, 1086 (1966).
[16] The notion of a cage plays an important role in the free volume theory of the glass transition. See, e.g., M. H. Cohen and D. Turnbull, J. Chem. Phys. **31**, 1164 (1959).
[17] The breakdown of no-slip under high stress was first seen in [8] for contact lines and in J. Koplik and J. R. Banavar, Phys. Fluids A **7**, 3118 (1995) in the context of corner flows in the sliding plate problem for a single fluid.